Chapter 3

The Thermal Stratification of the Extratropical Troposphere

Tapio Schneider

3.1. Introduction

Phillips's (1956) foundational paper on the general circulation of the atmosphere contains a list "of the most striking features of the atmosphere, calling for explanation." The first feature on the list is the "general increase of entropy (potential temperature) with height and the existence of the stratosphere," or, in other words, the thermal stratification of the atmosphere and the existence of the tropopause. Phillips's paper marks the beginning of general circulation studies as we know them now—experimenting with numerical models of various complexity to develop accounts of the maintenance and variability of observed atmospheric features. But despite decades of experimentation with general circulation models, the dynamics that determine the thermal stratification and the existence of the tropopause in the extratropics are only beginning to be understood.

One reason why our understanding of the extratropical thermal stratification is incomplete is that in quasigeostrophic models, such as that used by Phillips, the thermal stratification of the atmosphere is taken to be fixed. Quasigeostrophic models have formed the basis for studies of extratropical dynamics over the past decades and have led to some of the most important insights in dynamical meteorology (e.g., the theory of Rossby waves and baroclinic instability). But because they do not allow dynamics to affect the thermal stratification, quasigeostrophic models are poorly suited for studying the processes that determine the thermal stratification. With today's computational resources, however, we are in a position to study the maintenance and variability of the extratropical thermal stratification by systematic experimentation with general circulation models that are not based on quasigeostrophic assumptions.

This chapter discusses the dynamical mechanisms responsible for the maintenance and variability of the extratropical thermal stratification and tropopause in the zonal mean. Figure 3.1 shows the zonal-mean temperature lapse rate of Earth's atmosphere for boreal winter and summer. The zonal-mean lapse rate in the free

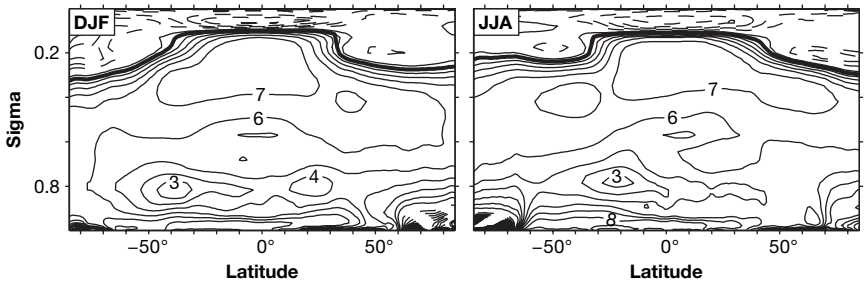

FIGURE 3.1. Zonal-mean temperature lapse rate $-\partial_z T$ ($\mathrm{K\,km^{-1}}$) for the DJF and JJA seasons according to reanalysis data for the years 1980–2001 provided by the European Centre for Medium-Range Weather Forecasts (ERA-40 data; see Uppala et al. 2005). Negative contours are dashed. The thick line marks the tropopause, determined as a $2\,\mathrm{K\,km^{-1}}$ isoline of the lapse rate. The vertical coordinate is pressure normalized by surface pressure, $\sigma = p/p_s$.

troposphere is relatively uniform (about $6.5\,\mathrm{K\,km^{-1}}$) and varies only weakly with season—observations that motivated the assumption of a fixed thermal stratification in quasigeostrophic theory. Regions of smaller lapse rate (statically more stable stratification) are seen near the surface in the subtropics and in high latitudes, particularly in winter. At the tropopause, the lapse rate decreases, in many regions to zero or less, marking the transition from the troposphere to the more stably stratified stratosphere.

What distinguishes the troposphere and stratosphere kinematically is that the bulk of the entropy the atmosphere receives by the heating at the surface is redistributed within the troposphere, whereas only a small fraction of it reaches the stratosphere. In fluid-dynamical parlance, the troposphere is the caloric boundary layer of the atmosphere; the tropopause is the top of this boundary layer. The question of what determines the thermal stratification is the question of what determines the dynamical equilibrium between radiative processes and dynamical entropy transport. If one accepts as an observational fact that the redistribution of the entropy received at the surface is largely confined to a well-defined boundary layer, the troposphere, the height of the tropopause can be determined as in classical boundary-layer theories: as the minimum height up to which the entropy redistribution must extend for the flow to satisfy large-scale constraints such as energy and momentum balance.

Section 3.2 discusses the general form of large-scale constraints on the thermal stratification and tropopause height, arising from radiative and dynamical considerations. Sections 3.3–3.5 discuss dynamical constraints that respectively take slantwise moist convection, moist convection coupled to baroclinic eddies, and baroclinic eddies as central for determining the thermal stratification and tropopause height. Section 3.6 presents simulations with an idealized general circulation model (GCM) that show that an atmosphere can have different dynamical regimes distinguishable according to whether convection or baroclinic eddies dominate the entropy redistribution between surface and tropopause. And section 3.7 concludes this chapter with a discussion of the results presented and of open questions.

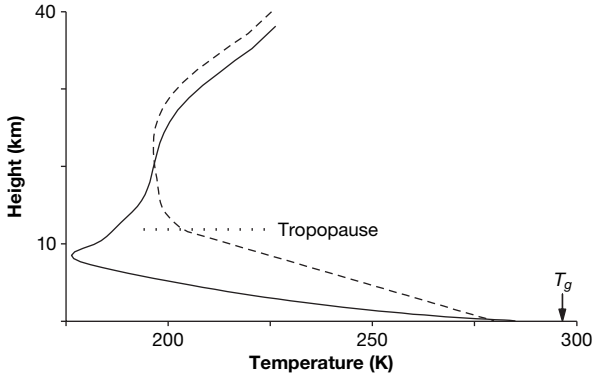

FIGURE 3.2. Temperature in radiative equilibrium (solid line) and in dynamical equilibrium with fixed tropospheric lapse rate $\Gamma = 6.5\,\mathrm{K\,km^{-1}}$ (dashed line). The arrow marks the ground temperature in radiative equilibrium, which is greater than the surface air temperature ($T_g \approx 297\,\mathrm{K}$, $T_s \approx 285\,\mathrm{K}$). The ground temperature in dynamical equilibrium is taken to be equal to the surface air temperature ($T_g = T_s = 280\,\mathrm{K}$). (Calculations courtesy Paul O'Gorman.)

3.2. Radiative and Dynamical Constraints

Held (1982) suggested distinguishing between radiative and dynamical constraints on the thermal stratification and tropopause height. Radiative constraints express the balance of incoming and outgoing radiant energy fluxes in atmospheric columns, plus any dynamical energy flux divergences in the columns. Dynamical constraints express balance conditions based on dynamical considerations, such as that moist convection maintains the thermal stratification close to a moist adiabat (see chapter 7 in this volume) or that baroclinic eddy fluxes satisfy balance conditions derived from the mean entropy and zonal momentum balances.

In the simplest model of dynamical equilibrium in an atmospheric column, going back to the concept of radiative-convective equilibrium (cf. Gold 1909; Milne 1922; Manabe and Strickler 1964; Manabe and Wetherald 1967), the dynamical constraint determines a constant tropospheric lapse rate and the radiative constraint determines the tropopause height that is consistent with the lapse rate and with a boundary condition, for example, a given surface temperature. Given a tropospheric lapse rate Γ and a surface air temperature T_s, taken to be equal to the ground temperature T_g, the radiative constraint determines the tropopause height H_t as the minimum height z at which the temperature profile $T_s - \Gamma z$ matches a radiative equilibrium temperature profile extending from the height H_t upward (cf. Held 1982; Thuburn and Craig 2000). Figure 3.2 shows such a dynamical equilibrium temperature profile with fixed tropospheric lapse rate and a corresponding radiative equilibrium temperature profile, computed with the column radiation model of the National Center for Atmospheric Research (Kiehl et al. 1996). In dynamical equilibrium, the tropospheric lapse rate is taken to be $\Gamma = 6.5\,\mathrm{K\,km^{-1}}$, and the ground and surface air temperatures are taken to

be $T_g = T_s = 280$ K. Following Thuburn and Craig (2000), the relative humidity is taken to be constant (50% relative to saturation over liquid water), subject to the constraint that the specific humidity in the stratosphere does not increase with height. Typical midlatitude concentrations are specified for other absorbers. Radiative effects of clouds are ignored, the surface albedo is 0.1, and the solar irradiance incident at the top of the atmosphere is taken to be $260\,\mathrm{W\,m^{-2}}$, a value about 15% lower than typical annual-mean irradiances in midlatitudes to compensate for the missing albedo of clouds. In radiative equilibrium, the absorber concentrations, solar irradiance at the top of the atmosphere, and albedo are taken to be the same as in dynamical equilibrium, but the ground and surface air temperatures are determined by the conditions of radiative equilibrium, rather than being specified as a boundary condition as in dynamical equilibrium. The dynamical equilibrium profile implies dynamical cooling in the lower troposphere and dynamical warming in the upper troposphere, associated with heat transport, for example, by convection or by baroclinic eddies. Above the tropopause, the dynamical equilibrium is a purely radiative equilibrium.

In radiative-convective equilibrium, the outgoing longwave radiant flux is equal to that in radiative equilibrium (where it is equal to the absorbed solar flux); that is, convection redistributes enthalpy only vertically. Unlike in radiative-convective equilibrium, in the dynamical equilibrium in Fig. 3.2 the outgoing longwave flux is not equal to that in radiative equilibrium. The outgoing longwave fluxes for the radiative and dynamical equilibrium profiles in Fig. 3.2 are $228\,\mathrm{W\,m^{-2}}$ and $239\,\mathrm{W\,m^{-2}}$, respectively, implying a net flux of enthalpy into the atmospheric column in dynamical equilibrium relative to radiative equilibrium. This implied enthalpy flux may be associated, for example, with convergence of meridional eddy enthalpy fluxes or with fluxes across the lower boundary of the atmosphere. An additional constraint is necessary to relate the temperature profiles in radiative and dynamical equilibrium to each other uniquely. The additional constraint can be an energy-balance condition at the surface, relating the surface temperature to meridional enthalpy fluxes and radiant fluxes.

Figure 3.3 shows the tropopause height determined according to the radiative constraint as a function of tropospheric lapse rate and surface temperature. As in Fig. 3.2 and in similar calculations by Thuburn and Craig (2000), the ground and surface air temperatures are taken to be equal, the relative humidity is taken to be constant, subject to the constraint that the specific humidity does not increase with height, and the concentrations of absorbers other than water vapor are taken to be fixed at typical midlatitude values. Figure 3.3 shows that for fixed lapse rate, the tropopause height increases with increasing surface temperature; for fixed surface temperature, the tropopause height increases with decreasing lapse rate (cf. Thuburn and Craig 2000).

The dependence of tropopause height on surface temperature and tropospheric lapse rate can be understood qualitatively by considering a semigray atmosphere (transparent to solar radiation and gray for longwave radiation) with an optically thin stratosphere. The stratosphere, according to the radiative constraint, is assumed to

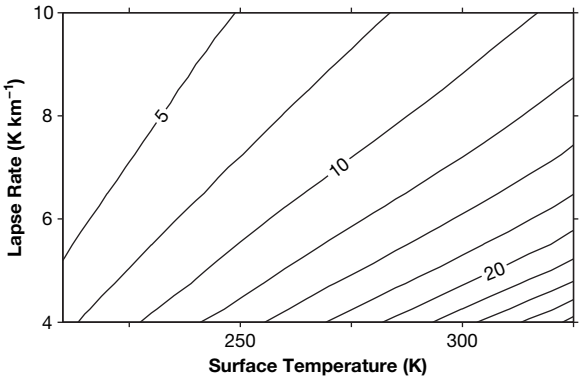

FIGURE 3.3. Tropopause height (km) determined according to the radiative constraint as a function of tropospheric lapse rate and surface temperature, with fixed relative humidity. Parameters and concentrations of absorbers other than water vapor as in Fig. 3.2. (Calculations courtesy Paul O'Gorman.)

be in radiative equilibrium. For a semigray atmosphere, the condition for radiative equilibrium in the two-stream approximation is $B = (U + D)/2$, where $B = \sigma_b T^4$ is the black-body emittance with Stefan-Boltzmann constant σ_b, and U and D are upwelling and downwelling fluxes of longwave radiant energy (Goody and Yung 1989, chapter 9). If the stratosphere is optically thin, the downwelling longwave flux D in it can be neglected, implying $B \approx U/2$ at the tropopause and in the stratosphere. It follows that the upwelling longwave flux U in an optically thin stratosphere in radiative equilibrium is approximately constant, equal to the outgoing longwave flux, and dependent only on properties of the troposphere (Thuburn and Craig 2000). The stratosphere is approximately isothermal, with a temperature $T_t \approx (U/2\sigma_b)^{1/4}$ that matches the tropospheric temperature profile $T_s - \Gamma z$ at the tropopause height $H_t = (T_s - T_t)/\Gamma$. In terms of the emission temperature T_e and of the emission height $H_e = (T_s - T_e)/\Gamma$ at which the tropospheric temperature is equal to the emission temperature, the upwelling longwave flux at the tropopause is $U \approx \sigma_b T_e^4$, the tropopause temperature is $T_t \approx \alpha T_e$ with $\alpha = 2^{-1/4} \approx 0.84$ (a relation going back to Schwarzschild [1906]), and the tropopause height is

$$H_t \approx (1 - \alpha)\frac{T_s}{\Gamma} + \alpha H_e. \qquad [3.1]$$

If the emission height is fixed, the tropopause height increases with increasing surface temperature and with decreasing lapse rate. The rate of increase of tropopause height with surface temperature, $\partial H_t/\partial T_s$, decreases with increasing lapse rate; the rate of decrease of tropopause height with lapse rate, $-\partial H_t/\partial\Gamma$, increases with increasing surface temperature and decreasing lapse rate, qualitatively as seen in Fig. 3.3.[1] In the radiative transfer model underlying Fig. 3.3, however, the emission height is not fixed but varies with water vapor concentrations, among other factors. Increasing the surface temperature while keeping the relative humidity and lapse rate fixed increases

water vapor concentrations and with them the emission height (see, e.g., Held and Soden 2000), which, according to the estimate (3.1), strengthens the dependence of tropopause height on surface temperature. Similarly, decreasing the lapse rate while keeping the relative humidity and surface temperature fixed increases water vapor concentrations above the surface, which increases the emission height and, according to the estimate (3.1), likewise strengthens the dependence of tropopause height on lapse rate. Such water vapor feedbacks account, for example, for the nonlinearity of the increase of tropopause height with surface temperature seen in Fig. 3.3 (cf. Thuburn and Craig 1997). To be sure, the assumption of a semigray atmosphere with an optically thin stratosphere is not quantitatively accurate for the radiative transfer model underlying Figs. 3.2 and 3.3. For example, absorption of solar radiation by ozone affects the radiative balances near the tropopause. But the tropopause height estimate (3.1) based on this assumption correctly describes the qualitative dependence of tropopause height on surface temperature and lapse rate and represents a rough quantitative estimate. Using representative midlatitude values for surface temperature $T_s = 280\,\mathrm{K}$, lapse rate $\Gamma = 6.5\,\mathrm{K\,km^{-1}}$, and emission height $H_e = 4\,\mathrm{km}$ gives the tropopause height $H_t = 10\,\mathrm{km}$, which is roughly consistent with the dynamical equilibrium profile in Fig. 3.2 and with the height of the observed extratropical tropopause in Fig. 3.1.

In GCM simulations, radiative constraints of the kind illustrated in Fig. 3.3 account latitude-by-latitude for variations of the extratropical zonal-mean tropopause height with surface temperature and with mean tropospheric lapse rate (Thuburn and Craig 1997, 2000). An exception are polar latitudes with strong temperature inversions near the surface (Fig. 3.1). There, the tropospheric thermal stratification is not well approximated by a constant lapse rate, and the radiative constraint needs to be modified. Taking the lapse rate to be constant, however, was merely done for simplicity. The radiative constraint can easily be modified by replacing the temperature profiles with constant lapse rates by families of temperature profiles with more complicated vertical structures. The way in which the tropopause height is determined given a tropospheric temperature profile and a boundary condition remains unaffected. The essential assumption remains that the stratosphere is approximately in radiative equilibrium. Although Earth's stratosphere is not in radiative equilibrium (there is a stratospheric circulation), the deviations from radiative equilibrium are small enough to be negligible in a first approximation of the height of the extratropical tropopause.

Given the surface temperature and a tropospheric lapse rate, or a different boundary condition and a more complicated tropospheric temperature profile, we can thus determine the tropopause height. In the Tropics, it is well established that moist convection dominates the entropy redistribution between surface and tropopause and maintains the thermal stratification in the interior troposphere close to a moist adiabat (see, e.g., Stone and Carlson [1979], Xu and Emanuel [1989], and chapter 7 in this volume). This provides a dynamical constraint on the tropical thermal stratification and tropopause height. The radiative constraint determines the tropical tropopause height

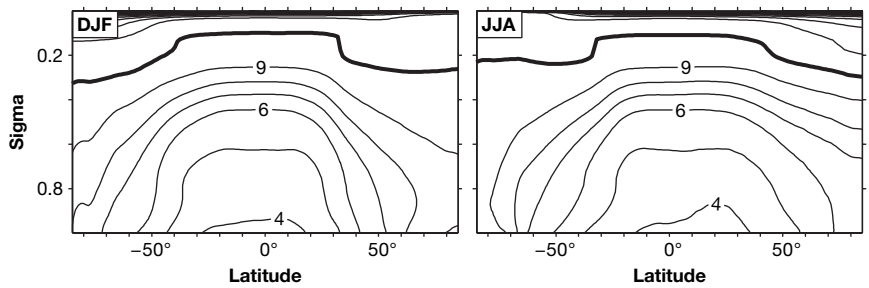

FIGURE 3.4. Zonal-mean moist adiabatic temperature lapse rate (K km^{-1}) according to ERA-40 data for 1980–2001. The thick line marks the tropopause.

as the minimum height up to which the moist adiabat and entropy redistribution by moist convection must extend so that the atmosphere above the tropopause can be approximately in radiative equilibrium.[2] The difficulty in accounting for the extratropical thermal stratification and tropopause height has its roots in the lack of dynamical constraints of comparable simplicity for the extratropics.

For a closed theory, we need two constraints in addition to the radiative constraint to relate the three unknowns: tropopause height, surface temperature, and tropospheric lapse rate or temperature profile. Here we take the surface temperature as given, returning to the question of what determines it in section (3.7), and discuss dynamical constraints relating it to the tropopause height and to the tropospheric lapse rate or temperature profile.

3.3. Slantwise Convection

As in the Tropics, moist convection maintains the thermal stratification close to a moist adiabat in some extratropical regions, for example in continental regions in summer. In the zonal mean and particularly in winter, however, comparison of the lapse rate (Fig. 3.1) with the moist adiabatic lapse rate (Fig. 3.4) shows that the extratropical lower troposphere is more stably stratified than a moist adiabat (Stone and Carlson 1979). At least in winter, mechanisms other than or in addition to moist convection appear to determine the extratropical thermal stratification and tropopause height.

Even when the atmosphere is stable with respect to vertical displacements, displacements along slanted surfaces may be unstable with respect to moist symmetric instability (Bennetts and Hoskins 1979; Emanuel 1983a, 1983b). The ensuing slantwise convection may play a role in determining the thermal stratification and tropopause height. Consider inviscid and reversible-adiabatic axisymmetric displacements of a tube of air that extends around a latitude circle and is embedded in a steady balanced flow. The tube is assumed to be thin, so that its displacements do not modify the pressure field of the environment. In inviscid axisymmetric displacements, the tube conserves

its absolute angular momentum per unit mass about the axis of planetary rotation, $m = (\Omega a \cos\phi + u) a \cos\phi$ in the approximation of the atmosphere as a thin spherical shell with radius a, angular velocity of planetary rotation Ω, latitude ϕ, and eastward wind component u. In reversible-adiabatic displacements, the tube conserves its entropy, with entropy understood as saturated moist entropy where condensation/freezing occurs. If, during an upward displacement along a possibly slanted surface on which the angular momentum m of the environment is constant, a tube of air encounters a region with entropy smaller than that of the tube, the tube becomes positively buoyant relative to its environment (assuming that buoyancy fluctuations are proportional to entropy fluctuations), and the displacement is convectively unstable. The tube can continue to move inviscidly upward along the angular momentum surface; slantwise convection ensues. Similarly, if, during a poleward displacement along a surface on which the entropy of the environment is constant (a moist isentrope), a tube of air encounters a region with angular momentum greater than that of the tube, the displacement is inertially unstable. The tube can continue to move adiabatically poleward along the isentrope; slantwise convection likewise ensues. Ordinary convective and inertial instabilities are special cases of moist symmetric instability in barotropic flows, in which angular momentum surfaces are vertical and moist isentropes are horizontal. The concept of slantwise convection unifies inertial and buoyancy forces and inertial and convective instabilities.

If angular momentum decreases poleward horizontally and if moist entropy increases upward vertically so that the flow is stable with respect to ordinary convective and inertial instabilities, the flow may nonetheless be unstable with respect to slantwise convection if, somewhere in the atmosphere, the slope of moist isentropes is steeper than or equal to the slope of angular momentum surfaces (Holton 2004, chapter 9; Emanuel 1994, chapter 12). Slantwise convection may occur if there is positive available potential energy for slantwise convection (Emanuel 1983b), which slantwise convection, possibly generating three-dimensional turbulent flows, would reduce by bringing entropy and angular momentum surfaces closer to alignment (Thorpe and Rotunno 1989). In a statistical equilibrium, one would expect that slantwise convection leads to an atmospheric state that is nearly neutral (cf. analogous considerations for ordinary convection in chapter 7 in this volume). In a neutral state, entropy and angular momentum surfaces are aligned, that is, temperature lapse rates along angular momentum surfaces are moist adiabatic. If slantwise convection were to determine the static stability of the extratropical atmosphere, the alignment of entropy and angular momentum surfaces would provide a dynamical constraint on the tropopause height and thermal stratification. The dynamical constraint would relate the temperature lapse rate to the specific (or relative) humidity and to the surface temperature and its derivatives, which, through thermal wind balance, determine the vertical wind shear and thus the slope of angular momentum surfaces.

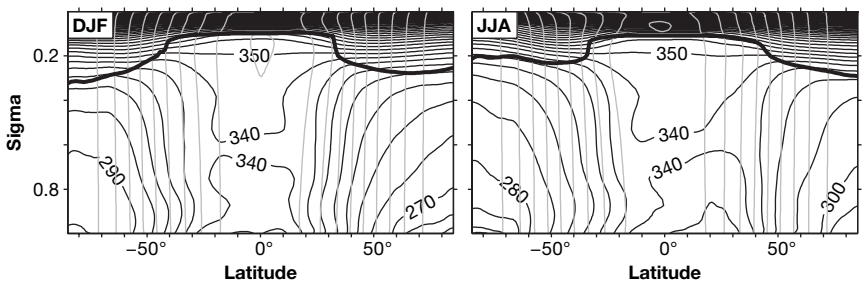

FIGURE 3.5. Saturation equivalent potential temperature (black, contour interval 10 K) and absolute angular momentum m (gray, contour interval $0.1\Omega a^2$) according to ERA-40 data for 1980–2001. The thick line marks the tropopause.

Ascending regions of extratropical cyclones are observed to be nearly neutral with respect to slantwise convection, suggesting that slantwise convection may occur there, with the displaced tube of air extending along a front, rather than around a latitude circle, and with the angular momentum to be considered correspondingly changed (Emanuel 1983b, 1988). But analyses are lacking that would establish the frequency and large-scale effects of slantwise convection in baroclinic eddies. Figure 3.5 shows zonal-mean moist adiabats (saturation equivalent potential temperature surfaces) and angular momentum surfaces calculated from reanalysis data. The mean stratification of the interior tropical troposphere is close to a moist adiabat. In summer in the Northern Hemisphere midlatitudes ($\sim 45^\circ$N), the mean stratification appears to be nearly neutral with respect to slantwise or ordinary moist convection. Higher latitudes and the Southern Hemisphere midlatitudes, in the zonal mean, appear to be stable with respect to slantwise or ordinary moist convection. However, slantwise convection, if it occurs, is a mesoscale phenomenon that is typically neither resolved nor parameterized in GCMs, so reanalysis data have to be used cautiously in establishing the potential importance of slantwise convection for the extratropical thermal stratification and tropopause height. More detailed analyses with different data may yield different results. And even if it is not a dominant process for the zonal-mean stratification, slantwise convection may still play a role regionally, for example, over continents in summer.

3.4. Moist Convection Coupled to Baroclinic Eddies

Moist processes such as moist convection and latent-heat release in large-scale condensation doubtlessly influence the extratropical static stability and tropopause height, likely as processes that are coupled to baroclinic eddies. The dynamics of baroclinic eddies in the presence of moisture, however, are poorly understood. The linear stability, nonlinear life cycles, and turbulent statistically steady states of moist baroclinic eddies

have been investigated in several studies, using models idealized to various degrees and with various ways of coupling moist processes to eddy dynamics (e.g., Mak 1982; Bannon 1986; Emanuel et al. 1987; Gutowski et al. 1992; Fantini 1993; Lapeyre and Held 2004). But there is no general theory accounting for the scales of baroclinically unstable waves in the presence of moisture, or for the relative importance of dry and moist processes in statistically steady states of baroclinic eddies.

Absent a general theory, Juckes (2000) proposed heuristic arguments for how moist convection coupled to baroclinic eddies may determine the extratropical thermal stratification. Moist convection in baroclinic eddies occurs preferentially in regions of low static stability—in the warm sectors of cyclones. To the extent that moist convection reaches the tropopause and prevents the stratification from becoming significantly less stable than a moist adiabat, the minimum of the bulk moist stability $\Delta_{ve} = \theta_{et} - \theta_{es}$, the equivalent potential temperature difference between tropopause (θ_{et}) and surface (θ_{es}), is approximately zero. Juckes assumes that the distribution of bulk moist stabilities in baroclinic eddies is well characterized by this minimum (zero) and the standard deviation, and that the temporal- and zonal-mean bulk moist stability $\bar{\Delta}_{ve} = \bar{\theta}_{et} - \bar{\theta}_{es}$ can be estimated as the minimum plus a multiple of the standard deviation,

$$\bar{\Delta}_{ve} \sim \min(\Delta_{ve}) + d\,\mathrm{std}(\Delta_{ve}), \qquad [3.2]$$

where d is an empirical factor. (For this assumption to result in a predictive theory, the empirical factor d needs to be universal, holding for a range of standard deviations. It is unclear whether this is an adequate assumption for distributions of bulk moist stabilities. For example, it is generally not an adequate assumption for log-normal distributions, according to which one might expect bulk moist stabilities to be distributed. It would be an adequate assumption for exponential distributions.) Juckes assumes fluctuations of bulk moist stability to be generated by approximately adiabatic meridional advection of equivalent potential temperature at the tropopause and at the surface by baroclinic eddies, such that the standard deviation scales as

$$\mathrm{std}(\Delta_{ve}) \sim L_e |\partial_y \overline{\theta}_e^p|, \qquad [3.3]$$

where L_e is an eddy length scale (or the width of the storm track) and $\partial_y \overline{\theta}_e^p$ is the mean meridional equivalent potential temperature gradient at constant pressure. (Juckes actually proposed that the standard deviation scales with the potential temperature gradient in place of the equivalent potential temperature gradient; however, in the presence of moisture, it is equivalent potential temperature rather than potential temperature that is materially conserved in adiabatic displacements, so using the equivalent potential temperature gradient appears to be preferable.) Juckes proposes that the equivalent potential temperature gradient is to be evaluated at a midtropospheric pressure level. If the standard deviation of bulk moist stability is dominated by near-surface fluctuations of equivalent potential temperature, however, it may be more appropriate to evaluate the

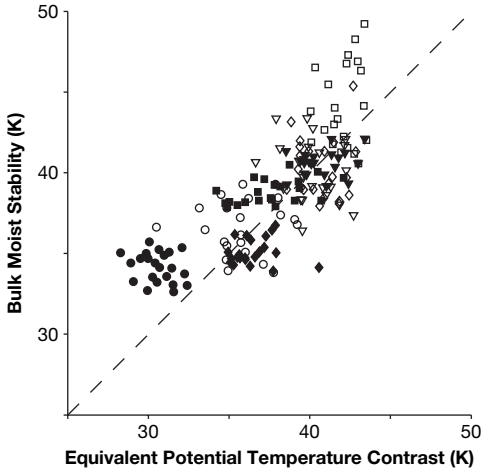

FIGURE 3.6. Extratropical mean bulk moist stabilities $\bar{\Delta}_{ev}$ and meridional equivalent potential temperature contrasts $dL_e|\partial_y\overline{\theta}_e^{\sigma}|$ according to ERA-40 data for 1980–2001. The length scale dL_e was chosen to be constant ($0.9a$ with Earth's radius a). The bulk stabilities and equivalent potential temperature gradients are seasonal and zonal averages over latitudes between 35° and 65° in the Northern and Southern Hemisphere, respectively, with the equivalent potential temperature gradient evaluated at the midtropospheric level $\sigma = 0.5$ (cf. Juckes 2000). Bulk moist stabilities are equivalent potential temperature differences between the tropopause and the near-surface level $\sigma = 0.9$. Each plotting symbol corresponds to a year and a season (squares: DJF; diamonds: MAM; circles: JJA; triangles: SON). Filled symbols represent Northern Hemisphere averages; open symbols represent Southern Hemisphere averages.

equivalent potential temperature gradient near the surface. Combining the estimates (3.2) and (3.3) and assuming that the minimum bulk moist stability is approximately zero, Juckes obtains the estimate

$$\bar{\Delta}_{ve} \sim dL_e|\partial_y\overline{\theta}_e^{p}|, \qquad [3.4]$$

which relates the mean bulk moist stability to the meridional equivalent potential temperature contrast $dL_e|\partial_y\overline{\theta}_e^{p}|$.[3]

Figure 3.6, similar to Fig. 6 of Juckes (2000) but with equivalent potential temperature gradients at a sigma level in place of potential temperature gradients at a pressure level, shows the relation between extratropical mean bulk moist stabilities and meridional equivalent potential temperature contrasts for different seasons and different years according to reanalysis data. The length scale dL_e was chosen to be constant (eddy length scales do not vary strongly interannually or seasonally in Earth's atmosphere). Consistent with Juckes's arguments, there is a positive correlation between seasonal

variations of bulk moist stabilities and meridional equivalent potential temperature contrasts. However, interannual variations of bulk moist stabilities and meridional equivalent potential temperature contrasts correlate less clearly. (These results do not change substantially if equivalent potential temperature contrasts are evaluated at different levels or if averages are taken over different extratropical latitude zones.)

If it can be more generally substantiated, and provided that an estimate of the length scale dL_e is available, the estimate (3.4) of the bulk moist stability provides a dynamical constraint on the extratropical tropopause height and thermal stratification, relating the temperature lapse rate and tropopause height, via the bulk moist stability, to the distribution of specific (or relative) humidity and to the meridional gradient of equivalent potential temperature. Although seasonal variations of the bulk moist stability are approximately linearly related to meridional equivalent potential temperature contrasts, it is an open question whether Juckes's proposed mechanism is indeed acting. The next section shows that dynamical constraints of a structure similar to that of the estimate (3.4) also arise from considerations of balance conditions on dry baroclinic eddies.

3.5. Baroclinic Eddies

Another dynamical constraint on the extratropical tropopause height and thermal stratification can be derived from balance conditions on baroclinic eddy fluxes without considering moist processes. To derive it, we need to estimate the vertical extent of the baroclinic entropy flux, which can modify the thermal stratification and tropopause height. The vertical extent of the baroclinic entropy flux will give a lower bound on the tropopause height. With the notion of the troposphere as the atmospheric layer within which entropy received at the surface is redistributed, the tropopause cannot lie below the height up to which significant baroclinic entropy fluxes extend, although it may lie above it, for example, if convective entropy fluxes extend to higher altitudes than baroclinic entropy fluxes. The vertical extent of the baroclinic entropy flux will depend on the meridional surface potential temperature gradient and on a measure of the tropospheric static stability, and will thus provide a dynamical constraint on the tropopause height and thermal stratification.

Since considerations of potential vorticity dynamics form a good basis of descriptions of the interaction between a mean flow and rapid, nearly adiabatic and inviscid fluctuations such as occur in baroclinic eddies, and since the potential vorticity flux has components only along isentropes, but not across isentropes (Haynes and McIntyre 1987, 1990), it is convenient to consider the interaction between the eddies and the mean flow and thermal stratification in isentropic coordinates. In isentropic coordinates, entropy fluxes correspond to mass fluxes along isentropes, so the question of the vertical extent of the baroclinic entropy flux is the question of the vertical extent of the baroclinic

mass flux along isentropes. Hence we need to discuss the structure of the mass flux along isentropes. We will ignore moist processes to investigate the extent to which dry extratropical dynamics alone can provide constraints on the thermal stratification and tropopause height and can provide limits to which any future theory accounting for moist processes must be reducible. The developments, based on a series of papers (Held and Schneider 1999; Schneider 2004, 2005; Schneider and Walker 2006), will be discussed in some detail to expose assumptions and approximations and to show how they differ from similar quasigeostrophic developments (cf. chapter 2 in this volume).

3.5.1. Balance Condition on Mean Mass Fluxes

The mean entropy balance in isentropic coordinates is equivalent to the mean mass balance,

$$\partial_y(\bar{\rho}_\theta \overline{v}^*) + \partial_\theta(\bar{\rho}_\theta \overline{Q}^*) = 0, \qquad [3.5]$$

where the meridional derivative is to be understood as a derivative at constant potential temperature θ, $Q = D\theta/Dt$ is the diabatic heating rate, and overbars denote temporal and zonal means: $\overline{(\cdot)}$ along isentropes, and $\overline{(\cdot)}^* = \overline{(\rho_\theta \cdot)}/\bar{\rho}_\theta$ along isentropes weighted by the isentropic density $\rho_\theta = -g^{-1}\partial_\theta p\, \mathcal{H}(\theta - \theta_s)$, where $\mathcal{H}(\cdot)$ is the Heaviside step function and the subscript s marks surface quantities (cf. Andrews et al. 1987, chapter 3). The Heaviside step function represents the convention that the isentropic density vanishes on isentropes "inside" the surface, that is, on isentropes with potential temperature $\theta < \theta_s(x, y, t)$ less than the instantaneous surface potential temperature. This convention ensures that the mean mass balance (3.5) holds throughout the flow domain in isentropic coordinates, including the surface layer of isentropes that, at any given latitude, sometimes intersect the surface (cf. Lorenz 1955). The meridional velocity $v = v_g + v_a$ can be decomposed into a geostrophic component v_g and an ageostrophic component v_a, where the geostrophic component in isentropic coordinates is $v_g = f^{-1}\partial_x M\, \mathcal{H}(\theta - \theta_s)$, with Montgomery streamfunction (dry static energy) $M = c_p T + gz$ and with the zonal derivative understood as a derivative at constant potential temperature. The Heaviside step function represents the convention that the geostrophic meridional velocity vanishes on isentropes inside the surface, a convention that is not necessary at this stage but will be used later. This decomposition leads to the alternative form of the mean mass balance

$$\partial_y(\bar{\rho}_\theta \overline{v}_g^*) = -\partial_\theta(\bar{\rho}_\theta \overline{Q}^*) - \partial_y(\bar{\rho}_\theta \overline{v}_a^*). \qquad [3.6]$$

Divergence of geostrophic mass fluxes along isentropes is balanced by vertical convergence of diabatic mass fluxes and by convergence of ageostrophic mass fluxes along isentropes.

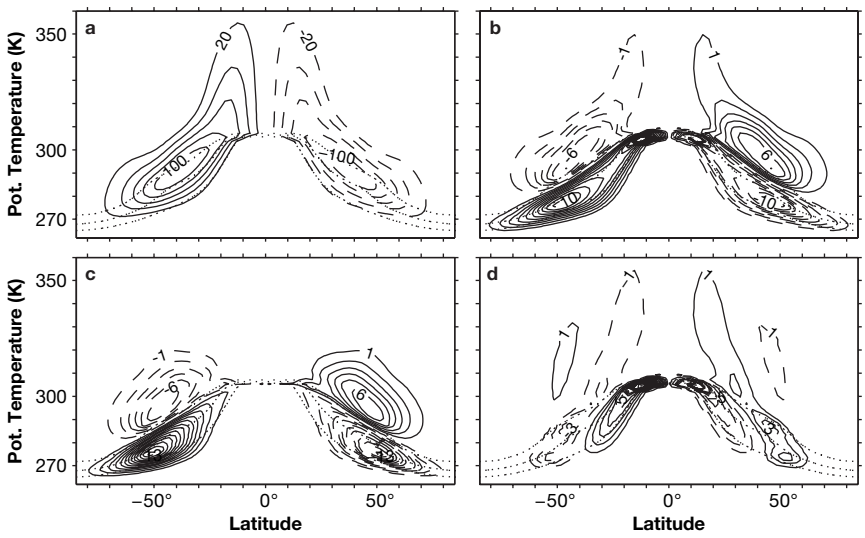

FIGURE 3.7. Isentropic mass fluxes in simulation with idealized GCM. (a) Mass flux streamfunction Ψ ($10^9\,\mathrm{kg\,s^{-1}}$); (b) meridional mass flux $\partial_\theta \Psi = 2\pi a \cos(\phi)\bar{\rho}_\theta \overline{v}^*$ with its (c) geostrophic and (d) ageostrophic components ($10^9\,\mathrm{kg\,s^{-1}\,K^{-1}}$). The dotted lines represent the 10%, 50%, and 90% isolines of the cumulative distribution of surface potential temperatures.

Figure 3.7, based on a simulation with the idealized GCM described in section 3.6, illustrates the mean mass balance in isentropic coordinates. The mass flux along and across isentropes can be represented by a streamfunction

$$\Psi(\phi, \theta) = 2\pi a \cos(\phi) \int_{\theta_b}^{\theta} \bar{\rho}_\theta \overline{v}^* \, d\theta',$$

where the potential temperature $\theta_b(\phi)$ is a nominal lower boundary, less than or equal to the lowest surface potential temperature that occurs at the latitude ϕ under consideration. The streamfunction forms an overturning cell in each hemisphere (Fig. 3.7a). Cross-isentropic rising corresponds to diabatic heating, and cross-isentropic sinking to diabatic cooling. Included in Fig. 3.7 are the 10%, 50%, and 90% isolines of the cumulative distribution of surface potential temperatures; that is, at any given latitude, the surface potential temperature is 10% of the time less than that indicated by the lowermost dotted line and 90% of the time less than that indicated by the uppermost dotted line. The 50% isoline, the median surface potential temperature, is approximately equal to the mean surface potential temperature. The 10% and 90% isolines can be taken as demarcating the *surface layer* of isentropes that, at any given latitude, sometimes intersect the surface. The meridional mass flux is equatorward near the surface, roughly in the surface layer, and poleward in the above-lying *interior atmosphere* (Fig. 3.7a, 3.7b). A large fraction of the equatorward mass flux at any given latitude occurs at potential temperatures below the median surface potential temperature, that is, in cold-air outbreaks (Held and Schneider 1999).

The geostrophic mass flux dominates the meridional mass flux in midlatitudes (Fig. 3.7c); the ageostrophic mass flux dominates in the Tropics (Fig. 3.7d). The geostrophic mass flux is poleward in the interior troposphere and equatorward in the surface layer. It is this geostrophic mass flux that is directly associated with baroclinic eddies; we need to estimate its vertical extent. The geostrophic mass flux along isentropes implies a net poleward and (because of the slope of isentropes) upward transport of entropy. The ageostrophic mass flux in the interior troposphere is poleward in the Tropics and equatorward in midlatitudes. It represents the upper branches of the Hadley cells and of the thermally indirect Ferrel cells. The ageostrophic mass flux in the surface layer is equatorward in the Tropics and poleward in midlatitudes. It represents the lower branches of the Hadley cells and of the Ferrel cells, or the Ekman transports due to the frictional stresses on surface easterlies in the Tropics and on surface westerlies in midlatitudes. The structures of the isentropic mass flux components in the idealized GCM resemble those of Earth's atmosphere (Johnson 1989).

To estimate the vertical extent of the baroclinic entropy flux, we need to estimate the vertical extent of the geostrophic mass flux along isentropes. Assume that the geostrophic mass flux extends up to a potential temperature θ_g above which it can be taken to vanish. Since the Coriolis force on the geostrophic mass flux in a layer balances the form drag or pressure drag on the layer, $f\bar{\rho}_\theta \overline{v}_g^* = \overline{\rho_\theta \partial_x M}$, the Coriolis force on the geostrophic mass flux integrated vertically up to potential temperature θ_g can be written as

$$f \int_{\theta_b}^{\theta_g} \bar{\rho}_\theta \overline{v}_g^* \, d\theta = \overline{p_s \partial_x z_s}^s - \overline{p \partial_x z}|_{\theta_g}, \qquad [3.7]$$

where $\overline{(\cdot)}^s$ denotes an average along the surface. The first term on the right-hand side is the surface pressure drag at mountains; the second term is the pressure drag of the above-lying atmosphere on the upper boundary of the layer extending from the nominal lower boundary θ_b to θ_g (Andrews 1983; Held and Schneider 1999; Koh and Plumb 2004). If the top of the atmosphere is taken as the upper boundary of the integration ($\theta_g \to \infty$), the second term on the right-hand side vanishes. The Coriolis force on the vertically integrated geostrophic mass flux in an atmospheric column balances the surface pressure drag at mountains. By splitting the integral to the top of the atmosphere into the sum of one segment from θ_b to θ_g, given by equation (3.7), and a second segment from θ_g to the top of the atmosphere, $f \int_{\theta_g}^{\infty} \bar{\rho}_\theta \overline{v}_g^* \, d\theta = \overline{p \partial_x z}|_{\theta_g}$, one sees that the assumption that the geostrophic mass flux is negligible above θ_g implies that the pressure drag $-\overline{p \partial_x z}|_{\theta_g}$ at the upper boundary of the layer extending from θ_b to θ_g is negligible. Therefore, it is consistent with our assumption of negligible geostrophic mass fluxes above θ_g to neglect the second term on the right-hand side of equation (3.7). Let us also assume that surface topography and the associated mountain pressure drag are negligible for estimating the vertical extent of the baroclinic entropy flux, such that the total pressure drag on the layer between θ_b and θ_g can be taken to vanish.

Then at each latitude the geostrophic mass flux integrates to zero over the layer (cf. Juckes et al. 1994),

$$\int_{\theta_b}^{\theta_g} \bar{\rho}_\theta \, \overline{v}_g^* \, d\theta \approx 0. \qquad [3.8]$$

To the extent that surface topography is negligible, the geostrophic mass flux alone forms a closed circulation, and we assume that this geostrophic circulation extends to potential temperature θ_g. From the perspective of the entropy or mass balance (3.6), this implies that the convergence of the ageostrophic mass flux vertically integrated up to potential temperature θ_g balances the diabatic heating at potential temperature θ_g. In the Tropics, the diabatic heating at the potential temperature θ_g up to which the geostrophic mass flux extends (if it is significant at all) is generally nonzero. Consequently, the convergence of the vertically integrated ageostrophic mass flux below that level is nonzero, and the ageostrophic mass flux extends to higher levels (cf. Fig. 3.7d). In midlatitudes, the diabatic heating at the potential temperature θ_g up to which the geostrophic mass flux extends may be close to zero and there may be no significant ageostrophic mass flux above that level if the atmosphere above that level is in an approximate radiative or radiative-convective equilibrium (for example, if the geostrophic mass flux extends to the tropopause and if the stratosphere, as in section 3.2, can be taken to be in an approximate radiative equilibrium).

3.5.2. Balance Condition on Eddy Fluxes

The balance condition (3.8) on the geostrophic mass flux along isentropes implies a balance condition on potential vorticity and surface potential temperature fluxes, fluxes of adiabatically approximately conserved quantities for which we can make closure assumptions to obtain an estimate of the vertical extent of the baroclinic entropy flux. To obtain the balance condition on eddy fluxes, we reformulate the geostrophic zonal momentum equation as a balance equation between the geostrophic mass flux and eddy fluxes.

If one expresses the planetary vorticity $f = \rho_\theta P_g$ as the product of isentropic density and of potential vorticity $P_g = f/\rho_\theta$ in the planetary-geostrophic limit, the definition of the geostrophic meridional velocity $v_g = f^{-1}\partial_x M \mathcal{H}(\theta - \theta_s)$ leads to the relation

$$f \, \overline{v}_g = \bar{\rho}_\theta \, \overline{v_g P_g}^* = \overline{\partial_x M \mathcal{H}},$$

with the shorthand $\mathcal{H} = \mathcal{H}(\theta - \theta_s)$ for the Heaviside step function. Decomposing the potential vorticity flux into mean and eddy components, with $\hat{(\cdot)} = (\cdot) - \overline{(\cdot)}^*$ denoting fluctuations about the density-weighted mean, and dividing by the mean potential

vorticity yields

$$\bar{\rho}_\theta \overline{v}^*_g = -\frac{\bar{\rho}_\theta \overline{\hat{v}_g \hat{P}_g}^*}{\overline{P_g}^*} + \frac{\overline{\partial_x M\mathcal{H}}}{\overline{P_g}^*}. \qquad [3.9]$$

The mean potential vorticity $\overline{P_g}^*$ on isentropes inside the surface involves the indefinite expression $\rho_\theta P_g = f\rho_\theta/\rho_\theta$ with $\rho_\theta = 0$, for which we adopt the convention $\rho_\theta/\rho_\theta = 1$, such that $\rho_\theta P_g = f$ on isentropes inside the surface as well as above the surface. (The developments in what follows depend crucially on this somewhat arbitrary convention; see Schneider [2005] for a rationale for this convention and Koh and Plumb [2004] and Schneider [2005] for alternative conventions.) With this convention, the mean potential vorticity is $\overline{P_g}^* = f/\bar{\rho}_\theta$ on isentropes in the surface layer as well as in the interior atmosphere. It then follows from the definition of the geostrophic meridional velocity that the second term on the right-hand side of the geostrophic mass flux decomposition (3.9) is, throughout the flow domain in isentropic coordinates, the mean component $\bar{\rho}_\theta \overline{v}_g$ of the geostrophic mass flux, and the first term, consequently, is the eddy component $\overline{\rho'_\theta v'_g}$ of the geostrophic mass flux,

$$\frac{\overline{\partial_x M\mathcal{H}}}{\overline{P_g}^*} = \bar{\rho}_\theta \overline{v}_g \quad \text{and} \quad -\frac{\bar{\rho}_\theta \overline{\hat{v}_g \hat{P}_g}^*}{\overline{P_g}^*} = \overline{\rho'_\theta v'_g},$$

with primes denoting fluctuations $(\cdot)' = (\cdot) - \overline{(\cdot)}$ about the isentropic mean. The relation between geostrophic eddy fluxes of potential vorticity and mass resembles similar relations in quasigeostrophic theory but, unlike in quasigeostrophic theory, in the present isentropic-coordinate framework it is only necessary to consider the planetary-geostrophic limit; it is not necessary to assume that fluctuations of the isentropic density are small. Also unlike in quasigeostrophic theory, the mean component $\bar{\rho}_\theta \overline{v}_g$ of the geostrophic mass flux does not vanish in the surface layer because the zonal average of the pressure gradient force per unit mass $-\partial_x M\mathcal{H}$ does not vanish but gives rise to a mean zonal pressure drag per unit mass, similar to the pressure drag at mountains appearing in the mean momentum balance in pressure or height coordinates (cf. Peixoto and Oort 1992, chapter 11). This mean surface pressure drag can contain topographic contributions, but it does not require topography; it is the mean zonal pressure drag per unit mass that the flow along isentropes experiences at intersections of isentropes with the surface, whether at topographic obstacles or at a flat surface (see Koh and Plumb [2004] and Schneider [2005] for details).

One obtains a balance condition on baroclinic eddy fluxes by integrating the geostrophic mass flux decomposition (3.9) from the nominal lower boundary θ_b to the potential temperature θ_g up to which the geostrophic mass flux along isentropes extends. The integral of the surface pressure drag term, which is only nonzero in the surface layer,

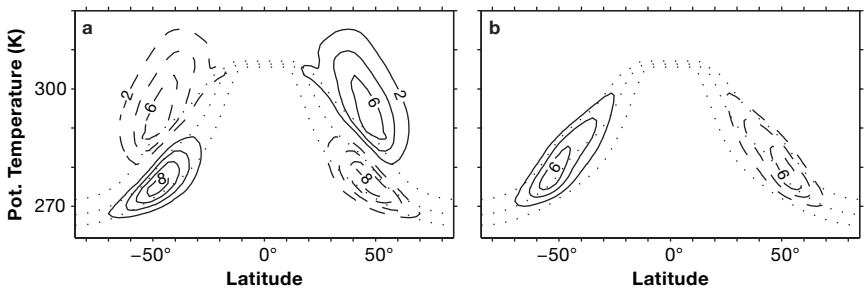

FIGURE 3.8. Components of geostrophic mass flux ($10^9 \mathrm{kg\,s^{-1}K^{-1}}$) along isentropes in the same GCM simulation as in Fig. 3.7. (a) Geostrophic eddy mass flux $\overline{\rho'_\theta v'_g} = -\bar{\rho}_\theta \overline{\hat{v}_g \hat{P}_g^*}/\overline{P_g^*}$; (b) geostrophic mean mass flux $\bar{\rho}_\theta \overline{v}_g = \overline{\partial_x M\mathcal{H}}/\overline{P_g^*}$. As in Fig. 3.7, the dotted lines represent the 10%, 50%, and 90% isolines of the cumulative distribution of surface potential temperatures.

becomes approximately

$$\int_{\theta_b}^{\theta_g} \frac{\overline{\partial_x M\mathcal{H}}}{\overline{P_g^*}}\, d\theta \approx -\bar{\rho}_\theta^0 \overline{v'_{gs}\theta'^s_s}, \qquad [3.10]$$

where $\bar{\rho}_\theta^0 = \bar{\rho}_\theta(\bar{\theta}_s)$ is the mean isentropic density at the temporal- and zonal-mean surface potential temperature $\bar{\theta}_s(\phi)$, and v'_{gs} is the geostrophic meridional eddy velocity at the surface (Schneider 2005). (Overbars now denote general temporal and zonal means, which are understood as means along isentropes if the argument depends on a vertical coordinate; primes denote fluctuations about surface or isentropic means.) Combining the constraint (3.8) on the geostrophic mass flux with the relations (3.9) and (3.10) yields a balance condition on eddy fluxes,

$$\int_{\theta_b}^{\theta_g} \bar{\rho}_\theta \overline{v}_g^*\, d\theta \approx -\int_{\theta_b}^{\theta_g} \frac{\bar{\rho}_\theta \overline{\hat{v}_g \hat{P}_g}^*}{\overline{P_g^*}}\, d\theta - \bar{\rho}_\theta^0 \overline{v'_{gs}\theta'^s_s} \approx 0. \qquad [3.11]$$

This balance condition makes manifest that the geostrophic mass flux along isentropes is directly associated with eddy fluxes of potential vorticity and of surface potential temperature. It states that, upon vertical integration, the geostrophic mass flux associated with the eddy flux of potential vorticity balances the geostrophic mass flux associated with the eddy flux of surface potential temperature. The balance condition is a statement of zonal momentum balance for baroclinic eddy fluxes and is the point of departure for estimating the vertical extent of the baroclinic entropy flux.

Figure 3.8 shows the eddy and mean components of the geostrophic mass flux along isentropes, or the components of the geostrophic mass flux along isentropes that are associated with the eddy fluxes of potential vorticity and, upon vertical integration, of surface potential temperature. In the interior atmosphere, only the geostrophic eddy mass flux, or the mass flux associated with the eddy flux of potential vorticity, contributes to the geostrophic mass flux along isentropes. In the surface layer,

both the eddy and mean components contribute to the geostrophic mass flux along isentropes, with contributions of the same sign and of the same order of magnitude (which can be shown to be generally the case; see Schneider [2005]). That both eddy and mean components (or eddy fluxes of potential vorticity and of surface potential temperature) contribute to the geostrophic mass flux in the surface layer contrasts with the representation of the near-surface mass flux in quasigeostrophic models, in which either the surface-layer potential vorticity flux (in continuously stratified models) or the surface potential temperature flux (in layer models) is neglected. See Schneider (2005) for reasons for this difference. The presence of surface-layer mass fluxes associated both with the potential vorticity flux and with the surface potential temperature flux is essential for the estimate of the vertical extent of the baroclinic entropy flux to be discussed below.

Qualitatively, the direction of the geostrophic mass flux can be understood by assuming that baroclinic eddies mix potential vorticity and surface potential temperature downgradient. The potential vorticity gradient $\partial_y \overline{P_g}^* = \beta/\bar{\rho}_\theta - f\partial_y\bar{\rho}_\theta/\bar{\rho}_\theta^2$ changes sign from the interior troposphere to the surface layer. It is generally positive in the interior troposphere because the Coriolis parameter increases poleward and the isentropic density usually decreases poleward along an isentrope. For sufficiently large surface potential temperature gradients, it is generally negative in the surface layer because the frequency with which an isentrope lies above the surface increases as one moves poleward along an isentrope, and so the mean isentropic density increases poleward along surface-layer isentropes. (The role the mean isentropic density plays here is similar to that of the layer thickness in quasigeostrophic two-layer models, in which the potential vorticity gradient, for a baroclinically unstable flow, likewise changes sign from the upper to the lower layer; see chapters 1 and 4 in this volume.) Consequently, eddy fluxes of potential vorticity are generally southward in the interior troposphere and northward in the surface layer and so are associated with poleward mass fluxes in the interior troposphere and with equatorward mass fluxes in the surface layer. Similarly, the eddy flux of surface potential temperature is generally poleward and hence is associated with a vertically integrated equatorward mass flux in the surface layer (Schneider 2005). Figure 3.9 illustrates the direction of the mass and eddy fluxes.

Having related the geostrophic mass flux to eddy fluxes of quantities that are approximately materially conserved in adiabatic fluctuations, we are now in a position to derive an estimate of the vertical extent of the geostrophic mass flux with the help of semi-empirical eddy flux closures that quantify the above qualitative arguments for the direction of eddy fluxes.

3.5.3. Vertical Extent of Baroclinic Entropy Flux and Supercriticality[4]

Assume that the eddy fluxes can be modeled as downgradient diffusive fluxes $\overline{\hat{v}_g \hat{P}_g}^* \sim -D\partial_y \overline{P_g}^*$ and $\overline{v'_{gs}\theta'^s_s} \sim -D\partial_y\tilde{\theta}_s$. Since it is not the planetary-geostrophic potential

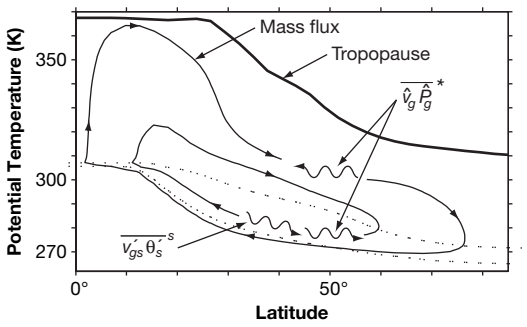

FIGURE 3.9. Sketch of isentropic mass flux and eddy fluxes (based on the idealized GCM simulation in Figs. 3.7 and 3.8). Streamlines are contours of the isentropic mass flux streamfunction shown in Fig. 3.7a. Wavy lines indicate eddy fluxes. The dotted lines represent the 10% and 90% isolines of the cumulative distribution of surface potential temperatures; that is, they demarcate the surface layer of isentropes within which, at any given latitude, the instantaneous surface potential temperature lies 80% of the time.

vorticity $P_g = f/\rho_\theta$ that is materially conserved in adiabatic fluctuations but the potential vorticity $P = (f + \zeta_\theta)/\rho_\theta$, which includes the relative vorticity ζ_θ normal to isentropes, the closure assumption for the planetary-geostrophic potential vorticity flux is tantamount to assuming that relative vorticity fluxes can be modeled separately from the planetary vorticity fluxes; that is, meridional fluxes of wave activity are either negligible or can be modeled separately from vertical fluxes of wave activity that are local in latitude (see chapter 1 in this volume for a discussion of conditions for the adequacy of diffusive eddy flux closures). If we further assume that the eddy diffusivity D may vary with latitude but is taken to have no essential vertical structure below the upper bound θ_g of the integration, the diffusivity drops out of the balance condition (3.11), and one obtains the estimate (Schneider and Walker 2006)

$$\bar{p}_s - \bar{p}_g \sim \frac{f}{\beta} \frac{\partial_y \bar{\theta}_s}{2\,\overline{\partial_p \theta}^s}. \qquad [3.12]$$

The difference between the mean surface pressure $\bar{p}_s$ and the mean pressure $\bar{p}_g = \bar{p}(\theta_g)$ up to which the baroclinic entropy flux extends depends on the meridional potential temperature gradient $\partial_y \bar{\theta}_s$ and on the static stability $-\overline{\partial_p \theta}^s$ at the surface (or immediately above a near-surface mixed layer). It does not depend explicitly, for example, on the eddy diffusivity and planetary rotation rate, although these parameters enter implicitly in determining the surface potential temperature gradient and the near-surface static stability. The pressure difference $\bar{p}_s - \bar{p}_g$ on the left-hand side arises from a vertical integration of the mean isentropic density $\bar{\rho}_\theta = -g^{-1}\overline{\partial_\theta p\,\mathcal{H}}$ in the potential-vorticity flux term in balance condition (3.11). The factor of two in the denominator on the right-hand side arises from the mean isentropic density $\bar{\rho}^0_\theta$ at the mean surface

potential temperature, which is about half a near-surface average of the isentropic density, since the isentrope with the mean surface potential temperature at any given latitude is about half the time inside the surface. Neglected in the estimate (3.12) is a term involving the slope of isentropes at the upper boundary θ_g—a term that is small in the extratropics of Earth's atmosphere if the upper boundary θ_g is identified with the tropopause (Schneider 2004; Schneider and Walker 2006).

In addition to the assumption of separability of potential vorticity flux components, the adequacy of the estimate (3.12) depends on the validity of the assumption that the eddy diffusivity has no essential vertical structure, implying vertically uniform mixing, in the pressure range over which the baroclinic entropy flux extends. Eddy diffusivities may be poorly defined or large in or near regions where the potential vorticity gradient vanishes (e.g., near the top of the surface layer, where the potential vorticity gradient changes sign). But as long as the potential vorticity fluxes in those regions vanish or are small, the structure of the eddy diffusivity in those regions is not essential for the adequacy of the estimate (3.12).

Consider the limiting cases of macroturbulence with weak nonlinear eddy–eddy interactions and macroturbulence with strong nonlinear eddy–eddy interactions. In strongly nonlinear macroturbulence, the inverse energy cascade to large horizontal and vertical scales would lead to barotropization of the energy-containing eddies (Smith and Vallis 2002). Therefore, since the energy-containing eddies are expected to dominate the advection of potential vorticity and surface potential temperature fluctuations (Held and Larichev 1996), the assumption of vertically uniform mixing is justifiable. In weakly nonlinear macroturbulence, mean flow properties such as the thermal stratification determine the vertical structure of baroclinic eddies. In Earth's atmosphere, however, the streamfunctions of the most unstable linear or weakly nonlinear waves vary only weakly in the pressure range over which baroclinic eddies redistribute entropy (Simmons and Hoskins 1976, 1977; Valdes and Hoskins 1988). To the extent that the vertical structure of the eddy diffusivity is similar to that of the streamfunction—the streamfunction scales with the product of an eddy length scale and an eddy velocity scale and so scales like an eddy diffusivity (Holloway 1986; Kushner and Held 1998)—the assumption of vertically uniform mixing thus remains plausible for rough estimates (cf. Held 1978). Thus, the estimate (3.12) can be expected to hold quite generally, at least in a scaling sense.[5]

A dynamical constraint on the extratropical thermal stratification and tropopause height is implied by the estimate (3.12) of the vertical extent of the baroclinic entropy flux. If the baroclinic entropy flux is strong and extends to the tropopause, possibly determining the height of the tropopause and the thermal stratification, the estimate (3.12) holds with the mean tropopause pressure $\bar{p}_t$ in place of $\bar{p}_g$. If baroclinic eddies are weak and the baroclinic entropy flux does not extend to the tropopause but the tropopause height is determined by other processes (such as radiation and convection), the pressure difference $\bar{p}_s - \bar{p}_g$ is less than the pressure difference between surface and

tropopause. That significant baroclinic entropy fluxes extend above the tropopause is inconsistent with the notion of the troposphere as the atmospheric layer within which entropy received at the surface is redistributed. Therefore, defining the bulk stability

$$\bar{\Delta}_v = -2\,\overline{\partial_p \theta}^s\,(\bar{p}_s - \bar{p}_t) \qquad [3.13]$$

and the supercriticality

$$S_c = -\frac{f}{\beta}\,\frac{\partial_y \bar{\theta}_s}{\bar{\Delta}_v}, \qquad [3.14]$$

a nondimensional measure of the slope of near-surface isentropes or a ratio of pressure ranges $S_c \sim (\bar{p}_s - \bar{p}_g)/(\bar{p}_s - \bar{p}_t)$, we conclude $S_c \lesssim 1$ (Schneider and Walker 2006). The supercriticality is less than one if the baroclinic entropy flux is shallower than the tropopause, as is typically the case in the Tropics; the supercriticality is approximately equal to one if the baroclinic entropy flux extends to the tropopause, as may be the case in the extratropics.

The constraint $S_c \lesssim 1$ provides a dynamical constraint on the thermal stratification and tropopause height, relating the temperature lapse rate near the surface and the tropopause height, via the bulk stability, to the meridional gradient of surface potential temperature and to the Coriolis parameter and its gradient. One may use a radiative constraint of the kind discussed in section 3.2 with a constant tropospheric lapse rate to obtain a first approximation of the tropopause height; for a more accurate account of the tropopause height, one should take the vertical structure of the thermal stratification into account, which the scaling arguments presented here do not provide.

For Earth-like atmospheres with approximately constant static stability $\partial_z \overline{\theta}^p$ and with an extratropical tropopause height somewhat greater than the scale height (with a quotient of extratropical tropopause height and scale height of about 1.5, as in Earth's atmosphere), the bulk stability in the supercriticality (3.14) is approximately equal to the potential temperature difference between tropopause and surface, $\bar{\Delta}_v \sim \bar{\theta}_t - \bar{\theta}_s$. (The decrease of density with height just compensates the factor of two in the bulk stability [3.13]; see Schneider and Walker [2006].) Hence, if baroclinic entropy fluxes determine the tropopause height ($S_c \sim 1$), the supercriticality constraint, aside from the ignored moist processes, differs from Juckes's dynamical constraint (3.4) primarily by the length scales that enter: $|f/\beta|$ for the supercriticality constraint and dL_e for Juckes's dynamical constraint. In midlatitudes, the length scale for the supercriticality constraint is approximately $|f/\beta| \approx a$, which, for Earth's atmosphere, is of the same order of magnitude as the length scale for Juckes's dynamical constraint ($dL_e = 0.9a$ was used in Fig. 3.6), so the two constraints are difficult to distinguish if the (equivalent) potential temperature gradient in Juckes's constraint scales similarly as the surface potential temperature gradient in the supercriticality constraint. If baroclinic entropy fluxes determine the tropopause height, the supercriticality constraint implies $\bar{\theta}_t - \bar{\theta}_s \sim a|\partial_y \bar{\theta}_s|$ in midlatitudes, which means that the potential temperature difference between

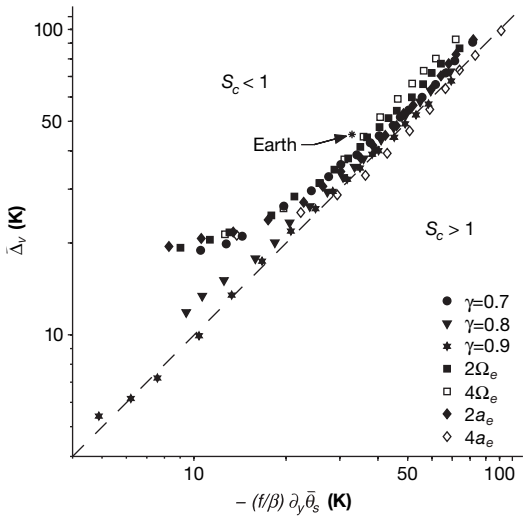

FIGURE 3.10. Extratropical bulk stability $\bar{\Delta}_v$ and scaled surface potential temperature gradient $-(f/\beta)\partial_y\bar{\theta}_s$ in dynamical equilibria of idealized GCM simulations. Included are results from simulations with terrestrial rotation rate Ω_e and radius a_e and with different convective lapse rates $\gamma\Gamma_d$ ($\gamma = 0.7, \ldots, 0.9$) and from simulations with twice and four times the rotation rate and radius of Earth. For each set of parameters, the figure shows a series of simulations obtained by varying the pole-equator surface temperature difference in radiative equilibrium. Displayed quantities are averages over extratropical baroclinic zones. The corresponding quantities for Earth's atmosphere (northern hemisphere annual mean according to ERA-40 data for 1980–2001) are shown for comparison. The dashed line represents supercriticality $S_c = 1$, with $S_c < 1$ above it and $S_c > 1$ below it. (Adapted from Schneider [2006].)

equator and pole is similar to that between tropopause and surface, as is indeed the case in Earth's atmosphere.

The supercriticality constraint depends on the assumption that the planetary vorticity gradient β is dynamically significant. It becomes singular in the limit $\beta \to 0$ (e.g., in the limit of infinite planet radius). It is unclear how baroclinic eddies would affect the thermal stratification and tropopause height if the energy-containing baroclinic eddies were so small compared with the planet radius that the planetary vorticity gradient β could effectively be set to zero.

3.6. Simulations with an Idealized GCM

Figure 3.10 shows the results of a test of dynamical constraints with an idealized GCM. The GCM is idealized in that, among other simplifications, radiative heating and cooling are represented by Newtonian relaxation of temperatures toward statically unstable

radiative-equilibrium states and in that it has no explicit hydrologic cycle. However, if a layer is statically unstable relative to a specified convective temperature lapse rate, a convection scheme mimics latent heat release by relaxing temperatures in that layer toward an enthalpy-conserving profile with the convective lapse rate. The convective lapse rate is $\gamma\Gamma_d$, where $\Gamma_d = g/c_p = 9.8\,\mathrm{K\,km^{-1}}$ is the dry adiabatic lapse rate and $\gamma \leq 1$ is a rescaling parameter. The scheme mimics the stabilizing effect of latent heat release in moist convection, with the implied latent heat release increasing with decreasing γ (see Schneider and Walker [2006] for a model description). The mean lapse rate of $6.5\,\mathrm{K\,km^{-1}}$ in Earth's tropical free troposphere corresponds to a rescaling parameter $\gamma = 0.66$.

The simulated circulations span a very wide range of possible planetary circulations, including circulations with multiple jets and belts of surface westerlies in each hemisphere. Consistent with the supercriticality constraint, all simulations in Fig. 3.10 condense onto the line $S_c \sim 1$ for sufficiently large surface potential temperature gradients. For small surface potential temperature gradients, there is a regime in which $S_c < 1$, in which baroclinic eddies are weak and the extratropical thermal stratification and tropopause height are determined by convection, similar to the tropical thermal stratification and tropopause height. In this regime, the extratropical lapse rate is approximately equal to the convective lapse rate (see Fig. 3.11, which shows dynamical-equilibrium lapse rates for representative simulations with convective lapse rate $0.9\Gamma_d = 8.8\,\mathrm{K\,km^{-1}}$). As the surface potential temperature gradient increases, the simulations approach the line $S_c \sim 1$ (Fig. 3.10). Consistent with the supercriticality constraint, the larger the convective lapse rate $\gamma\Gamma_d$, and hence the smaller the radiative-convective bulk stability, the smaller is the scaled surface potential temperature gradient $-(f/\beta)\partial_y \bar{\theta}_s$ at which the line $S_c \sim 1$ is reached. When the line $S_c \sim 1$ is reached, baroclinic entropy fluxes stabilize the extratropical thermal stratification and modify the tropopause height, such that the bulk stability $\bar{\Delta}_v$ increases in proportion with the scaled surface potential temperature gradient $-(f/\beta)\partial_y \bar{\theta}_s$. The stabilization of the thermal stratification is concentrated near the surface, but for sufficiently large surface temperature gradients or large convective lapse rates, the stratification throughout the troposphere is stabilized by eddies (Fig. 3.11). However, convection only ceases to provide a significant portion of the dynamical heating in the upper troposphere for larger convective lapse rates ($\gamma \geq 0.8$) and for the largest surface potential temperature gradients we simulated. It is potentially significant that, consistent with surface or near-surface quantities playing a prominent role in the theory of baroclinic entropy fluxes, the stratification stabilization is concentrated near the surface, similar to what is seen in Earth's atmosphere (cf. Fig. 3.1).

To obtain the close agreement between theory and simulations in Fig. 3.10, it is important that the potential temperature gradient near the surface is considered rather than a midtropospheric potential temperature gradient, such as would appear in quasigeostrophic baroclinic-adjustment constraints (cf. endnote 5 and chapter 2 in this volume). This difference between quasigeostrophic baroclinic-adjustment constraints

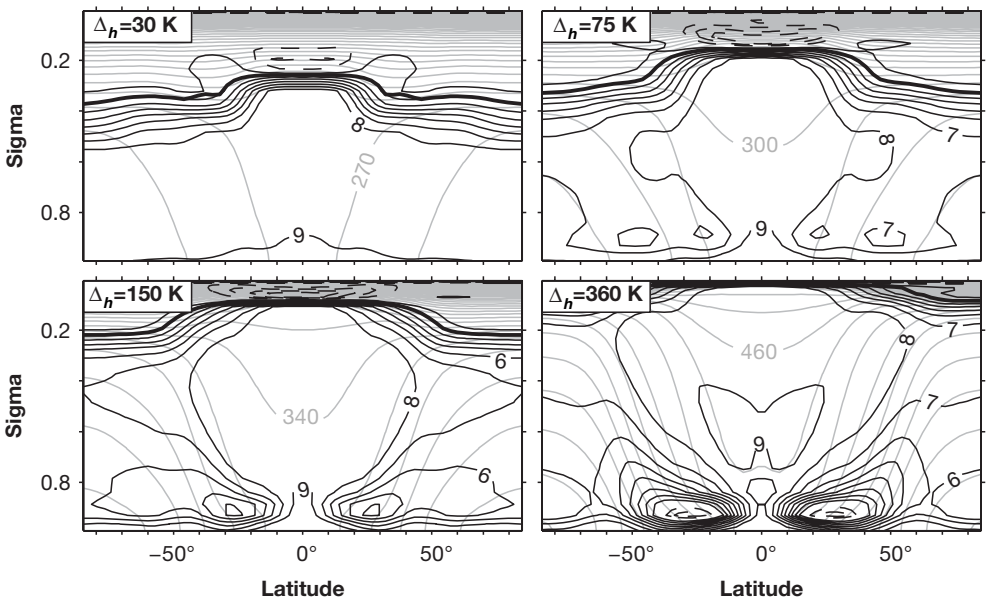

FIGURE 3.11. Zonal-mean temperature lapse rate, potential temperature, and tropopause in GCM simulations with terrestrial rotation rate and radius and convective lapse rate $0.9\Gamma_d = 8.8\,\mathrm{K\,km^{-1}}$. The pole-equator surface temperature difference in radiative equilibrium increases from $\Delta_h = 30\,\mathrm{K}$ in the upper left panel to $\Delta_h = 360\,\mathrm{K}$ in the lower right panel. The contour intervals are 10 K for potential temperature (gray) and $1\,\mathrm{K\,km^{-1}}$ for lapse rate (black, negative contours dashed). The heavy line marks the tropopause. The increase of tropopause height with Δ_h is primarily caused by an increase of the mean surface temperature with Δ_h, in accordance with the "radiative" constraint for the GCM. The increase of the mean surface temperature with Δ_h was necessary to make possible simulations with large Δ_h with physically realizable polar temperatures (Schneider and Walker 2006).

and the supercriticality constraint may, at least in part, be responsible for the lack of agreement Thuburn and Craig (1997) found between quasigeostrophic baroclinic-adjustment constraints and simulations with a complex GCM (additional complications due to comparing a theory that ignores moist processes with simulations with a GCM with a hydrologic cycle may also have contributed).

If Juckes's mechanism for determining the bulk stability were acting, one would expect to see systematic variations in bulk stability $\bar{\Delta}_v$ with convective lapse rate, since the convective lapse rate would change the minimum stability entering a dry variant of Juckes's mean bulk stability estimate (3.2). However, no such systematic variations are evident in Fig. 3.10. Instead, the bulk stabilities condense onto the line $S_c \sim 1$ irrespective of convective lapse rate. Similarly, extratropical angular momentum surfaces are generally steeper than neutral surfaces for convection with the specified convective lapse rate. There is no evidence for adjustment to a state that is neutral with respect to slantwise convection, as would not have been expected given that slantwise convection was neither resolved nor parameterized in the idealized GCM.

3.7. Discussion and Open Questions

The thermal stratification and tropopause height of the extratropical atmosphere can be maintained by at least two mechanisms, convection and baroclinic eddies. If the baroclinicity is small, convective entropy fluxes maintain the thermal stratification and tropopause height. To the extent that convection is in quasi-equilibrium with its large-scale environment, as it is in the simulations with the idealized GCM, the tropospheric lapse rate is equal to the convective lapse rate. In this convection-dominated regime, radiative constraints of the kind discussed in section 3.2 determine the tropopause height. If the baroclinicity is sufficiently large, baroclinic entropy fluxes stabilize the thermal stratification and modify the tropopause height, such that the supercriticality S_c does not significantly exceed one. In this eddy-dominated regime, radiative constraints likewise determine the tropopause height, with the lapse rate entering radiative constraints of the kind discussed in section 3.2 obtainable from the bulk stability and the tropopause height (that is, the radiative and dynamical constraints have to be solved simultaneously for the unknown lapse rate and tropopause height). The scaling theory for the vertical extent of the baroclinic entropy flux does not provide the vertical structure of the thermal stratification, which may have to be taken into account in radiative constraints if the lapse rate cannot be approximated by a constant. Whether slantwise convection plays a role in determining the thermal stratification and tropopause height was not addressed with the idealized GCM, since slantwise convection was neither resolved nor parameterized in the GCM. A variant of Juckes's mechanism, coupling baroclinic eddies and the parameterized convection of the idealized GCM, did not appear to be acting in the GCM.

The dynamical constraints discussed relate measures of the tropospheric lapse rate and the tropopause height via, for example, a bulk stability to the surface potential temperature and, in the case of dynamical constraints involving baroclinic eddies or slantwise convection, to the meridional gradient of surface potential temperature. In addition to the radiative constraint, a third constraint is necessary to obtain a closed theory for the tropopause height, thermal stratification, and surface temperature. This third constraint is given by an energy balance condition at the surface, which determines the surface temperature given the differential heating of the surface and a theory of how the eddy flux of surface (potential) temperature depends on other mean-field quantities. For example, if the eddy flux of surface potential temperature is related to mean-field quantities via a diffusive eddy flux closure, one needs to know how the eddy diffusivity depends on mean-field quantities. The supercriticality constraint does not depend on eddy diffusivities, but the meridional surface potential temperature gradient will depend on the eddy diffusivity. A theory of how the eddy flux of surface potential temperature depends on mean-field quantities is lacking, even leaving out moist processes, although the supercriticality constraint for baroclinic eddies points to how baroclinic-eddy

length and energy scales depend on mean-field quantities (Schneider and Walker 2006; Schneider 2006).

Given the prominence of large-scale condensation and moist convection in the extratropics of Earth's atmosphere, developing a theory of how moist processes affect baroclinic eddies is obviously important. The simulations with the idealized GCM with different convective lapse rates, mimicking different degrees of latent heating, suggest that the supercriticality constraint may be generalizable to moist atmospheres. The seasonal (Stone and Nemet 1996) and decadal (Schneider 2004) variability of Earth's atmosphere satisfies the constraint $S_c \lesssim 1$ or similar constraints (Stone 1978), despite considerable variability of the thermal structure. And the fundamental mechanism underlying the supercriticality constraint—macroturbulence reduces the surface potential temperature gradient and stabilizes the thermal stratification—also acts in a moist atmosphere. What is unclear, however, is what eddy flux closures are adequate in a moist atmosphere. The balance condition (3.11) is derived from the zonal momentum balance and thus also holds in a moist atmosphere. What may not hold in a moist atmosphere is the closure assumption of modeling the eddy fluxes of surface potential temperature and of potential vorticity along isentropes as diffusive fluxes. Other balance conditions, involving quantities that are materially conserved in moist adiabatic fluctuations, may be a more fruitful starting point for a theory taking moist processes into account.

Acknowledgments

I thank Chris Walker for carrying out the simulations shown in sections 3.5 and 3.6 and Paul O'Gorman for carrying out the radiative transfer calculations shown in section 3.2. Chris Walker and Paul O'Gorman also provided the ERA-40 data in a format that helped to produce the figures. Many of the presented results from my own work are based on collaborations, over several years, with Isaac Held and Chris Walker. I am grateful to Simona Bordoni, Kerry Emanuel, Robert Korty, Paul Kushner, Paul O'Gorman, and Adam Sobel for careful readings of and helpful comments on drafts of this chapter. Part of the material presented here is based upon work supported by the National Science Foundation under Grant No. 0450059.

Notes

1. Alternatively, in terms of the emission temperature, the tropopause height is $H_t \approx (T_s - \alpha T_e)/\Gamma$, an expression that, if the emission temperature and with it the tropopause temperature $T_t \approx \alpha T_e$ are proportional to the surface temperature, has the same qualitative dependence on surface temperature and lapse rate as the estimate (3.1) with fixed emission height. However, like the emission height, the emission temperature depends on water vapor concentrations and on other factors, and, although it increases with surface temperature, it is not proportional to the surface temperature.

2. In the Tropics the tropopause has been variously associated with the coldest point in an atmospheric column, with a critical value of temperature lapse rate, and with the height of the main convective outflow—different conventions that yield different tropopause heights. The radiative constraints discussed here can only be expected to account for the height up to which the bulk of the dynamical entropy redistribution extends, that is, in the Tropics approximately the height up to which significant entropy transport by moist convection extends (cf. Sarachik 1985). The radiative constraints do indeed seem to account for this height (Thuburn and Craig 1997; Highwood and Hoskins 1998). Depending on the radiative-equilibrium profile above this height, the coldest point in an atmospheric column may be considerably higher (Forster et al. 1997).

3. Similar considerations for slantwise convection coupled to baroclinic eddies lead to a minimum bulk moist stability that scales approximately with the product of equivalent and virtual potential temperature gradients, hence is quadratic in potential temperature gradients, with virtual potential temperature gradients arising from thermal wind balance and the slope of angular momentum surfaces (K. A. Emanuel, personal communication).

4. This subsection follows parts of Schneider and Walker (2006) closely, in some passages verbatim.

5. Estimates of the vertical extent of baroclinic eddy fluxes that structurally resemble (3.12) also arise within quasigeostrophic theory but differ from the estimate (3.12) fundamentally in the theoretical reasoning underlying them. For example, estimates resembling (3.12) arise if one considers the pressure range over which baroclinic eddies would need to modify the atmospheric thermal structure to stabilize it with respect to baroclinic instability (Lindzen and Farrell 1980). The estimate (3.12) differs from Lindzen and Farrell's and similar quasigeostrophic baroclinic-adjustment estimates (e.g., Stone 1978; Lindzen 1993) in that it neither presupposes nor implies that the atmosphere is neutral with respect to baroclinic instability. In contrast with quasigeostrophic baroclinic-adjustment estimates (cf. chapter 2 in this volume), neither potential vorticity nor surface potential temperature gradients are assumed to be small in the theory presented here; rather, they are sufficiently large that the mass fluxes associated with the eddy fluxes of potential vorticity and surface potential temperature, shown in Fig. 3.8, balance each other upon vertical integration. Moreover, the estimate (3.12) differs from quasigeostrophic baroclinic-adjustment estimates in that temperature gradients and static stabilities at the surface appear in place of the interior-atmosphere averages in the quasigeostrophic estimates. See Schneider (2004, 2005) and Schneider and Walker (2006) for a discussion of similarities and differences between the estimate (3.12) and quasigeostrophic estimates.

References

Andrews, D. G., 1983: A finite-amplitude Eliassen-Palm theorem in isentropic coordinates. *J. Atmos. Sci.*, **40**, 1877–1883.

Andrews, D. G., J. R. Holton, and C. B. Leovy, 1987: *Middle Atmosphere Dynamics*. International Geophysics Series, Vol. 40. Academic Press, 489 pp.

Bannon, P. R., 1986: Linear development of quasi-geostrophic baroclinic disturbances with condensational heating. *J. Atmos. Sci.*, **43**, 2261–2274.

Bennetts, D. A., and B. J. Hoskins, 1979: Conditional symmetric instability—a possible explanation for frontal rainbands. *Quart. J. Roy. Meteor. Soc.*, **105**, 945–962.

Emanuel, K. A., 1983a: The Lagrangian parcel dynamics of moist symmetric instability. *J. Atmos. Sci.*, **40**, 2368–2376.

Emanuel, K. A., 1983b: On assessing local conditional symmetric instability from atmospheric soundings. *Mon. Wea. Rev.*, **111**, 2016–2033.

Emanuel, K. A., 1988: Observational evidence of slantwise convective adjustment. *Mon. Wea. Rev.*, **116**, 1805–1816.

Emanuel, K. A., 1994: *Atmospheric Convection*. Oxford University Press, 580 pp.

Emanuel, K. A., M. Fantini, and A. J. Thorpe, 1987: Baroclinic instability in an environment of small stability to slantwise moist convection. Part I: Two-dimensional models. *J. Atmos. Sci.*, **44**, 1559–1573.

Fantini, M., 1993: A numerical study of two-dimensional moist baroclinic instability. *J. Atmos. Sci.*, **50**, 1199–1210.

Forster, P., R. S. Freckleton, and K. P. Shine, 1997: On aspects of the concept of radiative forcing. *Climate Dyn.*, **13**, 547–560.

Gold, E., 1909: The isothermal layer of the atmosphere and atmospheric radiation. *Proc. Roy. Soc. Lond. A*, **82**, 43–70.

Goody, R. M., and Y. L. Yung, 1989: *Atmospheric Radiation: Theoretical Basis*. 2nd ed. Oxford University Press, 519 pp.

Gutowski, W. J., Jr., L. E. Branscome, and D. A. Stewart, 1992: Life cycles of moist baroclinic eddies. *J. Atmos. Sci.*, **49**, 306–319.

Haynes, P. H., and M. E. McIntyre, 1987: On the evolution of vorticity and potential vorticity in the presence of diabatic heating and frictional or other forces. *J. Atmos. Sci.*, **44**, 828–841.

Haynes, P. H., and M. E. McIntyre, 1990: On the conservation and impermeability theorems for potential vorticity. *J. Atmos. Sci.*, **47**, 2021–2031.

Held, I. M., 1978: The vertical scale of an unstable baroclinic wave and its importance for eddy heat flux parameterizations. *J. Atmos. Sci.*, **35**, 572–576.

Held, I. M., 1982: On the height of the tropopause and the static stability of the troposphere. *J. Atmos. Sci.*, **39**, 412–417.

Held, I. M., and V. D. Larichev, 1996: A scaling theory for horizontally homogeneous, baroclinically unstable flow on a beta-plane. *J. Atmos. Sci.*, **53**, 946–952.

Held, I. M., and T. Schneider, 1999: The surface branch of the zonally averaged mass transport circulation in the troposphere. *J. Atmos. Sci.*, **56**, 1688–1697.

Held, I. M., and B. J. Soden, 2000: Water vapor feedback and global warming. *Annu. Rev. Energy Environ.*, **25**, 441–475.

Highwood, E. J., and B. J. Hoskins, 1998: The tropical tropopause. *Quart. J. Roy. Meteor. Soc.*, **124**, 1579–1604.

Holloway, G., 1986: Estimation of oceanic eddy transports from satellite altimetry. *Nature*, **323**, 243–244.

Holton, J. R., 2004: *An Introduction to Dynamic Meteorology*. International Geophysics Series, Vol. 88, 4th ed. Elsevier, 529 pp.

Johnson, D. R., 1989: The forcing and maintenance of global monsoonal circulations: An isentropic analysis. In B. Saltzman, Ed., *Advances in Geophysics*, Vol. 31, Academic Press, 43–304.

Juckes, M. N., 2000: The static stability of the midlatitude troposphere: The relevance of moisture. *J. Atmos. Sci.*, **57**, 3050–3057.

Juckes, M. N., I. N. James, and M. Blackburn, 1994: The influence of Antarctica on the momentum budget of the southern extratropics. *Quart. J. Roy. Meteor. Soc.*, **120**, 1017–1044.

Kiehl, J. T., J. J. Hack, G. B. Bonan, B. A. Boville, B. P. Briegleb, D. L. Williamson, and P. J. Rasch, 1996: Description of the NCAR Community Climate Model (CCM3). Tech. rep., National Center for Atmospheric Research, Boulder, Colorado. NCAR Technical Note NCAR/TN-420+STR, www.cgd.ucar.edu/cms/ccm3/TN-420.

Koh, T.-Y., and R. A. Plumb, 2004: Isentropic zonal average formulation and the near-surface circulation. *Quart. J. Roy. Meteor. Soc.*, **130**, 1631–1654.

Kushner, P. J., and I. M. Held, 1998: A test, using atmospheric data, of a method for estimating oceanic eddy diffusivity. *Geophys. Res. Lett.*, **25**, 4213–4216.

Lapeyre, G., and I. M. Held, 2004: The role of moisture in the dynamics and energetics of turbulent baroclinic eddies. *J. Atmos. Sci.*, **61**, 1693–1710.

Lindzen, R. S., 1993: Baroclinic neutrality and the tropopause. *J. Atmos. Sci.*, **50**, 1148–1151.

Lindzen, R. S., and B. Farrell, 1980: The role of the polar regions in global climate, and a new parameterization of global heat transport. *Mon. Wea. Rev.*, **108**, 2064–2079.

Lorenz, E. N., 1955: Available potential energy and the maintenance of the general circulation. *Tellus*, **7**, 157–167.

Mak, M., 1982: On moist quasigeostrophic baroclinic instability. *J. Atmos. Sci.*, **39**, 2028–2037.

Manabe, S., and R. F. Strickler, 1964: Thermal equilibrium of the atmosphere with a convective adjustment. *J. Atmos. Sci.*, **21**, 361–385.

Manabe, S., and R. T. Wetherald, 1967: Thermal equilibrium of the atmosphere with a given distribution of relative humidity. *J. Atmos. Sci.*, **24**, 241–259.

Milne, E. A., 1922: Radiative equilibrium: the insolation of an atmosphere. *Phil. Mag.*, **44**, 872–896.

Peixoto, J. P., and A. H. Oort, 1992: *Physics of Climate*. American Institute of Physics, 520 pp.

Phillips, N. A., 1956: The general circulation of the atmosphere: a numerical experiment. *Quart. J. Roy. Meteor. Soc.*, **82**, 123–164.

Sarachik, E. S., 1985: A simple theory for the vertical structure of the tropical atmosphere. *Pure Appl. Geophys.*, **123**, 261–271.

Schneider, T., 2004: The tropopause and the thermal stratification in the extratropics of a dry atmosphere. *J. Atmos. Sci.*, **61**, 1317–1340.

Schneider, T., 2005: Zonal momentum balance, potential vorticity dynamics, and mass fluxes on near-surface isentropes. *J. Atmos. Sci.*, **62**, 1884–1900.

Schneider, T., 2006: The general circulation of the atmosphere. *Ann. Rev. Earth Planet. Sci.*, **34**, 655–688.

Schneider, T., and C. C. Walker, 2006: Self-organization of atmospheric macroturbulence into critical states of weak nonlinear eddy–eddy interactions. *J. Atmos. Sci.*, **63**, 1569–1586.

Schwarzschild, K., 1906: Über das Gleichgewicht der Sonnenatmosphäre. *Nachrichten von der Königlichen Gesellschaft der Wissenschaften zu Göttingen. Math.-phys. Klasse*, **195**, 41–53.

Simmons, A. J., and B. J. Hoskins, 1976: Baroclinic instability on the sphere: Normal modes of the primitive and quasigeostrophic equations. *J. Atmos. Sci.*, **33**, 1454–1477.

Simmons, A. J., and B. J. Hoskins, 1977: Baroclinic instability on the sphere: Solutions with a more realistic tropopause. *J. Atmos. Sci.*, **34**, 581–588.

Smith, K. S., and G. K. Vallis, 2002: The scales and equilibration of midocean eddies: Forced-dissipative flow. *J. Phys. Oceanogr.*, **32**, 1699–1720.

Stone, P. H., 1978: Baroclinic adjustment. *J. Atmos. Sci.*, **35**, 561–571.

Stone, P. H., and J. H. Carlson, 1979: Atmospheric lapse rate regimes and their parameterization. *J. Atmos. Sci.*, **36**, 415–423.

Stone, P. H., and B. Nemet, 1996: Baroclinic adjustment: A comparison between theory, observations, and models. *J. Atmos. Sci.*, **53**, 1663–1674.

Thorpe, A. J., and R. Rotunno, 1989: Nonlinear aspects of symmetric instability. *J. Atmos. Sci.*, **46**, 1285–1299.

Thuburn, J., and G. C. Craig, 1997: GCM tests of theories for the height of the tropopause. *J. Atmos. Sci.*, **54**, 869–882.

Thuburn, J., and G. C. Craig, 2000: Stratospheric influence on tropopause height: The radiative constraint. *J. Atmos. Sci.*, **57**, 17–28.

Uppala, S. M., and coauthors, 2005: The ERA-40 reanalysis. *Quart. J. Roy. Meteor. Soc.*, **131**, 2961–3012.

Valdes, P. J., and B. J. Hoskins, 1988: Baroclinic instability of the zonally averaged flow with boundary layer damping. *J. Atmos. Sci.*, **45**, 1584–1593.

Xu, K.-M., and K. A. Emanuel, 1989: Is the tropical atmosphere conditionally unstable? *Mon. Wea. Rev.*, **117**, 1471–1479.